

Two-body B Meson Decays to η and η' : Observation of $B \rightarrow \eta K^*$

CLEO Collaboration

(June 14, 2018)

Abstract

In a sample of 19 million produced B mesons, we have observed the decays $B \rightarrow \eta K^*$ and improved our previous measurements of $B \rightarrow \eta' K$. The branching fractions we measure for these decay modes are $\mathcal{B}(B^+ \rightarrow \eta K^{*+}) = (26.4_{-8.2}^{+9.6} \pm 3.3) \times 10^{-6}$, $\mathcal{B}(B^0 \rightarrow \eta K^{*0}) = (13.8_{-4.6}^{+5.5} \pm 1.6) \times 10^{-6}$, $\mathcal{B}(B^+ \rightarrow \eta' K^+) = (80_{-9}^{+10} \pm 7) \times 10^{-6}$ and $\mathcal{B}(B^0 \rightarrow \eta' K^0) = (89_{-16}^{+18} \pm 9) \times 10^{-6}$. We have searched with comparable sensitivity for related decays and report upper limits for these branching fractions.

S. J. Richichi,¹ H. Severini,¹ P. Skubic,¹ A. Undrus,¹ S. Chen,² J. Fast,² J. W. Hinson,² J. Lee,² N. Menon,² D. H. Miller,² E. I. Shibata,² I. P. J. Shipsey,² V. Pavlunin,² D. Cronin-Hennessy,³ Y. Kwon,^{3,*} A.L. Lyon,³ E. H. Thorndike,³ C. P. Jessop,⁴ H. Marsiske,⁴ M. L. Perl,⁴ V. Savinov,⁴ D. Ugolini,⁴ X. Zhou,⁴ T. E. Coan,⁵ V. Fadeyev,⁵ Y. Maravin,⁵ I. Narsky,⁵ R. Stroynowski,⁵ J. Ye,⁵ T. Wlodek,⁵ M. Artuso,⁶ R. Ayad,⁶ C. Boulahouache,⁶ K. Bukin,⁶ E. Dambasuren,⁶ S. Karamnov,⁶ S. Kopp,⁶ G. Majumder,⁶ G. C. Moneti,⁶ R. Mountain,⁶ S. Schuh,⁶ T. Skwarnicki,⁶ S. Stone,⁶ G. Viehhauser,⁶ J.C. Wang,⁶ A. Wolf,⁶ J. Wu,⁶ S. E. Csorna,⁷ I. Danko,⁷ K. W. McLean,⁷ Sz. Márka,⁷ Z. Xu,⁷ R. Godang,⁸ K. Kinoshita,^{8,†} I. C. Lai,⁸ S. Schrenk,⁸ G. Bonvicini,⁹ D. Cinabro,⁹ L. P. Perera,⁹ G. J. Zhou,⁹ G. Eigen,¹⁰ E. Lipeles,¹⁰ M. Schmidtler,¹⁰ A. Shapiro,¹⁰ W. M. Sun,¹⁰ A. J. Weinstein,¹⁰ F. Würthwein,^{10,‡} D. E. Jaffe,¹¹ G. Masek,¹¹ H. P. Paar,¹¹ E. M. Potter,¹¹ S. Prell,¹¹ V. Sharma,¹¹ D. M. Asner,¹² A. Eppich,¹² J. Gronberg,¹² T. S. Hill,¹² D. J. Lange,¹² R. J. Morrison,¹² H. N. Nelson,¹² R. A. Briere,¹³ B. H. Behrens,¹⁴ W. T. Ford,¹⁴ A. Gritsan,¹⁴ H. Krieg,¹⁴ J. Roy,¹⁴ J. G. Smith,¹⁴ J. P. Alexander,¹⁵ R. Baker,¹⁵ C. Bebek,¹⁵ B. E. Berger,¹⁵ K. Berkelman,¹⁵ F. Blanc,¹⁵ V. Boisvert,¹⁵ D. G. Cassel,¹⁵ M. Dickson,¹⁵ P. S. Drell,¹⁵ K. M. Ecklund,¹⁵ R. Ehrlich,¹⁵ A. D. Foland,¹⁵ P. Gaidarev,¹⁵ L. Gibbons,¹⁵ B. Gittelman,¹⁵ S. W. Gray,¹⁵ D. L. Hartill,¹⁵ B. K. Heltsley,¹⁵ P. I. Hopman,¹⁵ C. D. Jones,¹⁵ D. L. Kreinick,¹⁵ M. Lohner,¹⁵ A. Magerkurth,¹⁵ T. O. Meyer,¹⁵ N. B. Mistry,¹⁵ C. R. Ng,¹⁵ E. Nordberg,¹⁵ J. R. Patterson,¹⁵ D. Peterson,¹⁵ D. Riley,¹⁵ J. G. Thayer,¹⁵ P. G. Thies,¹⁵ B. Valant-Spaight,¹⁵ A. Warburton,¹⁵ P. Avery,¹⁶ C. Prescott,¹⁶ A. I. Rubiera,¹⁶ J. Yelton,¹⁶ J. Zheng,¹⁶ G. Brandenburg,¹⁷ A. Ershov,¹⁷ Y. S. Gao,¹⁷ D. Y.-J. Kim,¹⁷ R. Wilson,¹⁷ T. E. Browder,¹⁸ Y. Li,¹⁸ J. L. Rodriguez,¹⁸ H. Yamamoto,¹⁸ T. Bergfeld,¹⁹ B. I. Eisenstein,¹⁹ J. Ernst,¹⁹ G. E. Gladding,¹⁹ G. D. Gollin,¹⁹ R. M. Hans,¹⁹ E. Johnson,¹⁹ I. Karliner,¹⁹ M. A. Marsh,¹⁹ M. Palmer,¹⁹ C. Plager,¹⁹ C. Sedlack,¹⁹ M. Selen,¹⁹ J. J. Thaler,¹⁹ J. Williams,¹⁹ K. W. Edwards,²⁰ R. Janicek,²¹ P. M. Patel,²¹ A. J. Sadoff,²² R. Ammar,²³ A. Bean,²³ D. Besson,²³ R. Davis,²³ I. Kravchenko,²³ N. Kwak,²³ X. Zhao,²³ S. Anderson,²⁴ V. V. Frolov,²⁴ Y. Kubota,²⁴ S. J. Lee,²⁴ R. Mahapatra,²⁴ J. J. O'Neill,²⁴ R. Poling,²⁴ T. Riehle,²⁴ A. Smith,²⁴ J. Urheim,²⁴ S. Ahmed,²⁵ M. S. Alam,²⁵ S. B. Athar,²⁵ L. Jian,²⁵ L. Ling,²⁵ A. H. Mahmood,^{25,§} M. Saleem,²⁵ S. Timm,²⁵ F. Wappler,²⁵ A. Anastassov,²⁶ J. E. Duboscq,²⁶ K. K. Gan,²⁶ C. Gwon,²⁶ T. Hart,²⁶ K. Honscheid,²⁶ D. Hufnagel,²⁶ H. Kagan,²⁶ R. Kass,²⁶ J. Lorenc,²⁶ T. K. Pedlar,²⁶ H. Schwarthoff,²⁶ E. von Toerne,²⁶ and M. M. Zoeller²⁶

¹University of Oklahoma, Norman, Oklahoma 73019

²Purdue University, West Lafayette, Indiana 47907

*Permanent address: Yonsei University, Seoul 120-749, Korea.

†Permanent address: University of Cincinnati, Cincinnati OH 45221

‡Permanent address: Massachusetts Institute of Technology, Cambridge, M A 02139.

§Permanent address: University of Texas - Pan American, Edinburg TX 785 39.

- ³University of Rochester, Rochester, New York 14627
- ⁴Stanford Linear Accelerator Center, Stanford University, Stanford, California 94309
- ⁵Southern Methodist University, Dallas, Texas 75275
- ⁶Syracuse University, Syracuse, New York 13244
- ⁷Vanderbilt University, Nashville, Tennessee 37235
- ⁸Virginia Polytechnic Institute and State University, Blacksburg, Virginia 24061
- ⁹Wayne State University, Detroit, Michigan 48202
- ¹⁰California Institute of Technology, Pasadena, California 91125
- ¹¹University of California, San Diego, La Jolla, California 92093
- ¹²University of California, Santa Barbara, California 93106
- ¹³Carnegie Mellon University, Pittsburgh, Pennsylvania 15213
- ¹⁴University of Colorado, Boulder, Colorado 80309-0390
- ¹⁵Cornell University, Ithaca, New York 14853
- ¹⁶University of Florida, Gainesville, Florida 32611
- ¹⁷Harvard University, Cambridge, Massachusetts 02138
- ¹⁸University of Hawaii at Manoa, Honolulu, Hawaii 96822
- ¹⁹University of Illinois, Urbana-Champaign, Illinois 61801
- ²⁰Carleton University, Ottawa, Ontario, Canada K1S 5B6
and the Institute of Particle Physics, Canada
- ²¹McGill University, Montréal, Québec, Canada H3A 2T8
and the Institute of Particle Physics, Canada
- ²²Ithaca College, Ithaca, New York 14850
- ²³University of Kansas, Lawrence, Kansas 66045
- ²⁴University of Minnesota, Minneapolis, Minnesota 55455
- ²⁵State University of New York at Albany, Albany, New York 12222
- ²⁶Ohio State University, Columbus, Ohio 43210

There has been considerable recent interest in charmless hadronic B decays, partly because of the observation of several of these decays [1–3], and partly because of their anticipated importance in understanding the phenomenon of CP violation. These decays are expected to proceed primarily through $b \rightarrow s$ loop (“penguin”) diagrams and $b \rightarrow u$ spectator diagrams. In Fig. 1 we show four such diagrams which may be expected to contribute to the decays involving isoscalar mesons which are the subject of this Letter. An earlier search [2] found a large rate for the decay $B \rightarrow \eta' K$, and set upper limits on other decays to two-body final states containing η or η' mesons. Recent effective Hamiltonian predictions [4,5] of the decay branching fractions of the $B \rightarrow \eta' K$ decay are still somewhat smaller than the measurement [2].

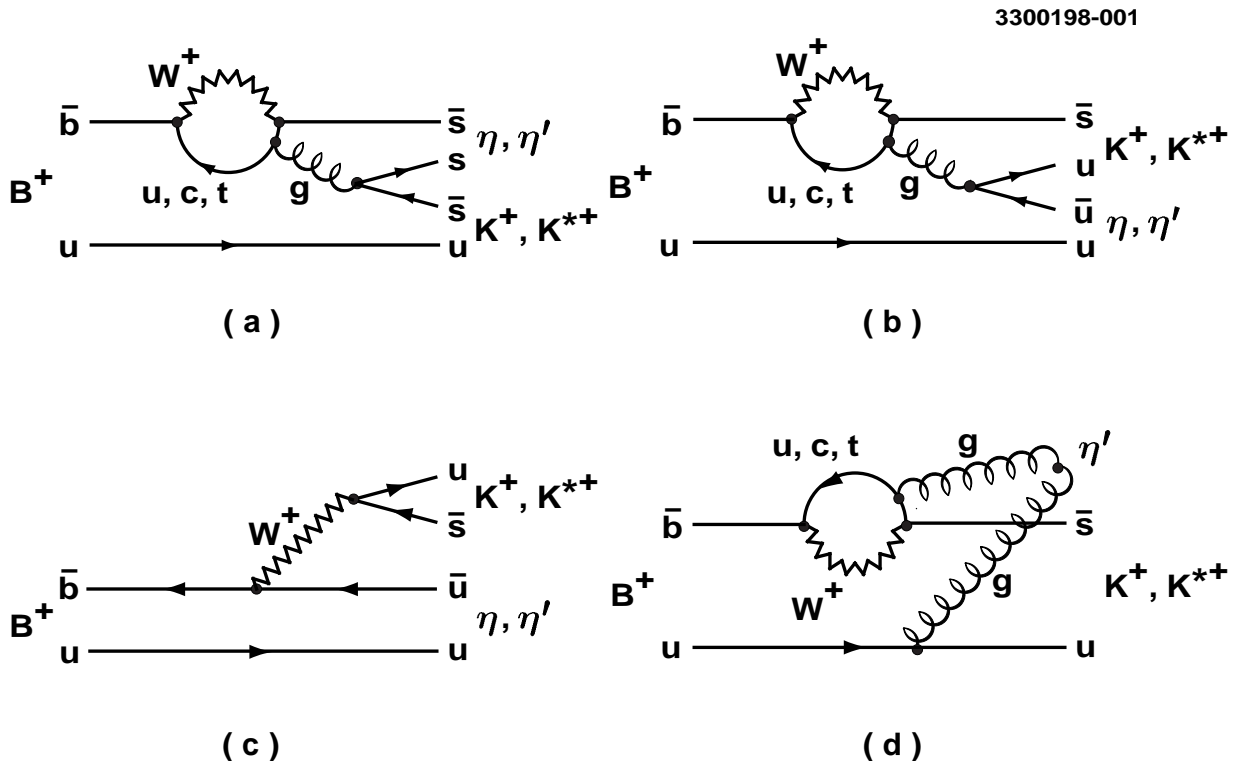


FIG. 1. Feynman diagrams describing the representative decays $B^+ \rightarrow \eta^{(\prime)} K^{(*)+}$: (a, b) internal penguins; (c) external spectator; (d) flavor-singlet penguin.

We present results of improved experimental searches for B meson decays to two-body final states containing η or η' mesons with the first observation of the decay $B \rightarrow \eta K^*$. These results are based on data collected with the CLEO II detector [6] at the Cornell Electron Storage Ring (CESR). The data sample corresponds to an integrated luminosity of 9.13 fb^{-1} for the reaction $e^+e^- \rightarrow \Upsilon(4S) \rightarrow B\bar{B}$, which in turn corresponds to $9.66 \times 10^6 B\bar{B}$ pairs [7]. To study background from continuum processes, we also collected 4.35 fb^{-1} of data at a center-of-mass energy below the threshold for $B\bar{B}$ production. These constitute the complete data sample from the CLEO II and CLEO II.V experiments, and the measurements we report here supersede our earlier results [2] from a subset of these data.

The CLEO II detector emphasizes precision charged particle tracking, with specific ionization (dE/dx) measurement, and high resolution electromagnetic calorimetry based on

CsI(Tl). Scintillators between the tracking chambers and calorimeter provide time-of-flight (TOF) information which we use in conjunction with dE/dx for particle identification (PID). The CLEO II.V configuration [8] differs in two respects: the replacement of an inner straw-tube drift chamber with a three-layer, double-sided-silicon vertex detector; and replacement of the 50:50 argon-ethane gas in the main drift chamber with a 60:40 helium-propane mixture.

We reconstruct charged pions and kaons, photons, and $\pi^+\pi^-$ pairs that intersect at a vertex displaced from the collision point (“vees” from $K_S^0 \rightarrow \pi^+\pi^-$). Candidate B decay tracks must meet specifications on the number of drift chamber measurements, goodness of fit, and consistency with an origin at the primary or particular secondary vertex. Candidate photons (from π^0 , η , and η' decays) must be isolated calorimeter clusters with a photon-like spatial distribution and energy deposition exceeding 30 MeV. In order to reject soft photon backgrounds, we require $\eta \rightarrow \gamma\gamma$ candidates to satisfy $|\cos\theta^*| < 0.97$, where θ^* is the center-of-mass decay angle relative to its flight direction. This cut is tightened to 0.90 for $\eta K^*/\rho$ channels to veto $B \rightarrow K^*\gamma$ background. We reject charged tracks and photon pairs having momentum less than 100 MeV/c. The photon from candidate $\eta' \rightarrow \rho\gamma$ decays is required to have an energy greater than 200 MeV, though this requirement is relaxed to 100 MeV for channels with relatively low background.

We fit photon pairs and vees kinematically to the appropriate combined mass hypothesis to obtain meson momenta. The reconstructed mass resolutions prior to the constraint are about 5–10 MeV (momentum dependent) for $\pi^0 \rightarrow \gamma\gamma$, 12 MeV for $\eta \rightarrow \gamma\gamma$, and 3 MeV for $K_S^0 \rightarrow \pi^+\pi^-$. We determine the expected signal distributions for these and other quantities needed in the analysis from a detailed GEANT based simulation of the CLEO detector [9] and studies of data for a variety of benchmark processes. In particular, we have determined the momentum and dE/dx resolutions in studies of $D^0 \rightarrow K^-\pi^+$ data events for track momenta greater than 2.0 GeV/c.

The primary means of identification of B meson candidates is through their measured mass and energy. The quantity ΔE is defined as $\Delta E \equiv E_1 + E_2 - E_b$, where E_1 and E_2 are the energies of the two B daughters (typically ~ 2.6 GeV) and E_b is the beam energy (5.29 GeV). The beam-constrained mass of the candidate is defined as $M \equiv \sqrt{E_b^2 - |\mathbf{p}|^2}$, where \mathbf{p} is the measured momentum of the candidate (typically $|\mathbf{p}| \sim 325$ MeV/c). We use the beam energy instead of the measured energy of the B candidate to improve the mass resolution by about one order of magnitude.

For vector-pseudoscalar decays of the B and the $\rho\gamma$ decay of the η' , we gain further discrimination from the helicity variable \mathcal{H} , the cosine of the vector meson’s rest frame two-body decay angle with respect to its flight direction, which reflects the spin alignment in the decay. The decay rate is proportional to \mathcal{H}^2 when the vector meson decays into two spinless daughters, and to $1 - \mathcal{H}^2$ for $\eta' \rightarrow \rho\gamma$. For modes in which one daughter is a single charged track, dE/dx measurements provide statistical discrimination between kaons and pions. With S_K and S_π defined as the deviations from nominal energy loss for the indicated particle hypotheses measured in standard deviations, the separation $S_K - S_\pi$ is about 1.7 (2.0) at 2.6 GeV/c for the CLEO II (II.V) samples.

The large background from continuum quark–antiquark ($q\bar{q}$) production can be reduced with event shape cuts. Because B mesons are produced almost at rest, the decay products of the $B\bar{B}$ pair tend to be isotropically distributed, while particles from $q\bar{q}$ production have

a more jet-like distribution. The angle θ_T between the thrust axis of the charged particles and photons forming the candidate B and the thrust axis of the remainder of the event is required to satisfy $|\cos \theta_T| < 0.9$. Continuum background is strongly peaked near 1 and signal is approximately flat for $|\cos \theta_T|$. We also form a multivariate discriminant (\mathcal{F}) [10] from the momentum scalar sum of charged particles and photons in nine cones of increasing polar angle around the thrust axis of the candidate, the angle of the thrust axis of the candidate, and the direction of \mathbf{p} with respect to the beam axis. We have checked the backgrounds from the dominant B decay modes ($b \rightarrow c$) by simulation, finding their contributions to the modes in this study to be generally quite small. Where appropriate we include this component in the fits described below.

The selection criteria for mass, energy, and event shape variables are chosen to include sidebands about the expected signal peaks. To extract event yields we perform unbinned extended maximum likelihood fits to the data [2]. Observables for each event include M , ΔE , \mathcal{F} , and (where applicable) resonance masses and \mathcal{H} . The number of events included in the fits ranges from ~ 100 to 20,000.

For B^+ decays [11] that have a primary daughter charged hadron (generically h^+) that can be either π^+ or K^+ , we fit both modes simultaneously, with the likelihood \mathcal{L} expanded so that the signal and background yields of both π^+ and K^+ are fit variables. The modes with a secondary vector decay involving h^+ ($K^* \rightarrow K^+\pi$ and $\rho \rightarrow \pi^+\pi$) also require special treatment. For these modes the momentum spectrum of h^+ is bimodal because of the forward-backward peaked \mathcal{H} distribution. We select independent K^* and ρ samples to fit according to the sign of \mathcal{H} . Events with $\mathcal{H} < 0$ in our sign convention have low momentum h^+ and are unambiguously separated by kinematics combined with PID information from dE/dx measurements. For the events with $\mathcal{H} > 0$ the separation is much smaller, so we fit both K^* and ρ yields simultaneously, using the K^* hypothesis for \mathcal{H} . In all cases involving two h^+ hypotheses, we include the normalized dE/dx observables S_π and S_K in the fit. For K^{*0} , we distinguish $K^+\pi^-$ from $K^-\pi^+$ candidates using dE/dx and TOF information. The kinematics and the definition of \mathcal{H} for these neutral decays causes $\sim 85\%$ of all $\rho^0 \rightarrow \pi^+\pi^-$ signal candidates to be assigned to the $\mathcal{H} > 0$ sample. All possible combinations are included except $K^{*0} \rightarrow K^0\pi^0$ (efficiency too small) and $\mathcal{H} > 0$ with low momentum π^0 for the $\eta' \rightarrow \rho\gamma$ channel (background too large).

The probability distribution functions (PDF) are constructed as products of functions of the observables. For signal the dependences on masses and energies are represented by Gaussian, double Gaussian, or Breit-Wigner functions, whose parameters are fixed in the fit. The background PDF contains signal-like peaking components in its resonance mass projections, to account for real resonances in the background, added to smooth components for combinatoric continuum. The smooth components are low-order polynomials, except that for M we use an empirical shape [12] that accounts for the phase space limit at $M = E_b$. The signal and background dependences of \mathcal{F} , S_K , and S_π are bifurcated Gaussian functions. We obtain the signal parameters from separate fits to simulated signal, and background parameters from fits to the below-threshold data sample. If the simulation estimate of background from $\Upsilon(4S)$ production is non-negligible, we add a term with a free fit variable to account for this as well.

Intermediate results for all of the B decay chains appear in Table I. Where relevant, the two \mathcal{H} hemispheres have been combined. We combine the samples from multiple secondary

decay channels by adding the $-2 \ln \mathcal{L}$ functions of branching fraction and extracting a value with errors or 90% confidence level (CL) upper limit from the combined distribution. The limit is the value of \mathcal{B} below which lies 90% of the integral of \mathcal{L} . In Table II we summarize the final results for these measurements with theoretical estimates [13]. The first error is statistical and the second systematic. The latter include systematic contributions from uncertainties in the PDFs [2], reconstruction efficiencies and selection requirements (~ 10 – 15%). We quote limits computed with efficiencies reduced by one standard deviation.

We have analyzed each of the decays without use of the likelihood fit, employing more restrictive cuts in each of the variables to isolate the signals. The results are consistent with those quoted above but with less precision.

The signals we find in both charge states of $B \rightarrow \eta K^*$ are first observations [11]: $\mathcal{B}(B^+ \rightarrow \eta K^{*+}) = (26.4_{-8.2}^{+9.6} \pm 3.3) \times 10^{-6}$ and $\mathcal{B}(B^0 \rightarrow \eta K^{*0}) = (13.8_{-4.6}^{+5.5} \pm 1.6) \times 10^{-6}$. The significance, defined as the number of standard deviations corresponding to the probability for a fluctuation from zero to our observed yield, is about 5 standard deviations for both. We show in Fig. 2 the projections of event distributions onto the M axis. A cut has been made to reject events with small values of signal \mathcal{L} , where for these purposes \mathcal{L} is calculated with M excluded. The signals appear as peaks at the B meson mass of 5.28 GeV in these plots. We also improve our previous measurements [2] of $B \rightarrow \eta' K$ with the full CLEO II/II.V data sample: $\mathcal{B}(B^+ \rightarrow \eta' K^+) = (80_{-9}^{+10} \pm 7) \times 10^{-6}$ and $\mathcal{B}(B^0 \rightarrow \eta' K^0) = (89_{-16}^{+18} \pm 9) \times 10^{-6}$. The M projections for these modes are also shown in Fig. 2.

Assuming equal decay rates of charged and neutral B mesons to $\eta^{(\prime)} K^{(*)}$, we combine the measured branching fractions [7]. We obtain $\mathcal{B}(B \rightarrow \eta' K) = (83_{-8}^{+9} \pm 7) \times 10^{-6}$ and $\mathcal{B}(B \rightarrow \eta K^*) = (18.0_{-4.3}^{+4.9} \pm 1.8) \times 10^{-6}$. We determine 90% CL upper limits for $\mathcal{B}(B \rightarrow \eta' K^*)$ and $\mathcal{B}(B \rightarrow \eta K)$ to be 22×10^{-6} and 5.2×10^{-6} , respectively, corresponding to central values of $(9.0_{-5.0}^{+6.7}) \times 10^{-6}$ and $(1.4_{-1.4}^{+2.2}) \times 10^{-6}$ with statistical and systematic errors combined. The pattern $\mathcal{B}(\eta K) < \mathcal{B}(\eta K^*) < \mathcal{B}(\eta' K)$ and $\mathcal{B}(\eta' K^*) < \mathcal{B}(\eta' K)$ is evident.

The observed branching fractions for $B \rightarrow \eta' K$ and $B \rightarrow \eta K^*$, in combination with the upper limits for the other modes in Table II and with recent measurements of $B \rightarrow K\pi$, $\pi\pi$ [14], $B \rightarrow \omega\pi$, $\rho\pi$ [15], and CP asymmetry in $B \rightarrow K\pi$, $\eta' K$, $\omega\pi$ [16] provide important constraints on the theoretical picture for these charmless hadronic decays. The effective Hamiltonian calculations [4,5,13] commonly used to account for the charmless hadronic B decays contain many uncertainties including form factors, light quark masses, CKM [17] angles and the QCD scale. A large ratio of $\mathcal{B}(B \rightarrow \eta' K, \eta K^*)$ to $\mathcal{B}(B \rightarrow \eta K, \eta' K^*)$, consistent with our measurements, was predicted qualitatively [18] in terms of interference of the two penguin diagrams in Fig. 1(a) and (b), constructive for $\eta' K$ and ηK^* and destructive for ηK and $\eta' K^*$. Most detailed calculations [4,5,13] predict a large branching fraction for the $B \rightarrow \eta' K$ modes (though usually smaller than the observed values), but no enhancement of $B \rightarrow \eta K^*$. Three recent analyses [19–21], all of which take guidance from charmless hadronic B decay data, show that the expectations for $B \rightarrow \eta K^*$ can easily be enhanced; the effective Hamiltonian calculations accomplish this by increasing the relevant form factor or decreasing the strange quark mass, the latter in accordance with recent lattice calculations [22]. These and previous calculations fall somewhat short of explaining the large rate for $B \rightarrow \eta' K$, suggesting that the solution may involve contributions that are unique to the η' meson.

We thank George Hou and Hai-Yang Cheng for many useful discussions. We gratefully ac-

knowledge the effort of the CESR staff in providing us with excellent luminosity and running conditions. This work was supported by the National Science Foundation, the U.S. Department of Energy, the Research Corporation, the Natural Sciences and Engineering Research Council of Canada, the A.P. Sloan Foundation, the Swiss National Science Foundation, and the Alexander von Humboldt Stiftung.

REFERENCES

- [1] CLEO Collaboration, R. Godang *et al.*, Phys. Rev. Lett. **80**, 3456 (1998).
- [2] CLEO Collaboration, B.H. Behrens *et al.*, Phys. Rev. Lett. **80**, 3710 (1998).
- [3] CLEO Collaboration, T. Bergfeld *et al.*, Phys. Rev. Lett. **81**, 272 (1998).
- [4] A. Ali, G. Kramer, and C.-D. Lu, Phys. Rev. D **59**, 014005 (1999).
- [5] Y.-H. Chen, H.-Y. Cheng, B. Tseng, and K.-C. Yang, hep-ph/9903453, March, 1999.
- [6] CLEO Collaboration, Y. Kubota *et al.*, Nucl. Instrum. Methods Phys. Res., Sec. A **320**, 66 (1992).
- [7] We assume the numbers of produced B^+B^- and $B^0\bar{B}^0$ events to be equal. The experimental uncertainty in the ratio is $\sim 10\%$.
- [8] T. Hill, Nucl. Instrum. Methods Phys. Res., Sec. A **418**, 32 (1998).
- [9] GEANT 3.15: R. Brun *et al.*, Report No. CERN DD/EE/84-1.
- [10] CLEO Collaboration, D.M. Asner *et al.*, Phys. Rev. D **53**, 1039 (1996).
- [11] Inclusion of the charge conjugate states is implied throughout this paper.
- [12] With $x \equiv M/E_b$ and ξ a parameter to be fit, $f(x) \propto x\sqrt{1-x^2} \exp[-\xi(1-x^2)]$ (H. Albrecht *et al.*, Phys. Lett. **B241**, 278 (1990); **254**, 288 (1991)).
- [13] For a full list of older theoretical predictions, see Ref. [2].
- [14] CLEO Collaboration, D. Cronin-Hennessy *et al.*, CLNS 99/1650, CLEO 99-18.
- [15] CLEO Collaboration, C.P. Jessop *et al.*, CLNS 99/1652, CLEO 99-19.
- [16] CLEO Collaboration, S. Chen *et al.*, CLNS 99/1651, CLEO 99-17.
- [17] M. Kobayashi and T. Maskawa, Prog. Theor. Phys. **49**, 652 (1973).
- [18] H. J. Lipkin, Phys. Lett. **B254**, 247 (1991).
- [19] M. Gronau and J. Rosner, hep-ph/9909478, 1999.
- [20] W.S. Hou, J.G. Smith, and F. Würthwein, hep-ex/9910014, 1999.
- [21] H-Y Cheng and K-C Yan, hep-ph/9910291, 1999.
- [22] S. Aoki, in Proceedings of the Symposium on Lepton and Photon Physics, Stanford, 1999 (to be published).

TABLE I. Intermediate results for final states listed in the first column, with the subscripts denoting secondary decays, including $\eta' \rightarrow \eta\pi^+\pi^-$ ($\eta\pi\pi$) with $\eta \rightarrow \gamma\gamma$ ($\gamma\gamma$), $\eta' \rightarrow \rho\gamma$ ($\rho\gamma$), and $\eta \rightarrow \pi^+\pi^-\pi^0$ (3π). The remaining columns give event yield from the fit, reconstruction efficiency ϵ , total efficiency with secondary branching fractions \mathcal{B}_s , and the resulting B decay branching fraction \mathcal{B} , with statistical error only.

Final state	Fit events	$\epsilon(\%)$	$\epsilon\mathcal{B}_s(\%)$	$\mathcal{B}(10^{-6})$
$\eta'_{\eta\pi\pi}K^+$	$39.6^{+7.0}_{-6.4}$	27	4.7	88^{+16}_{-14}
$\eta'_{\rho\gamma}K^+$	61^{+11}_{-10}	29	8.7	72^{+13}_{-12}
$\eta'_{\eta\pi\pi}K^0$	$9.2^{+3.6}_{-2.9}$	24	1.4	67^{+26}_{-21}
$\eta'_{\rho\gamma}K^0$	$29.6^{+7.0}_{-6.2}$	28	2.9	105^{+25}_{-22}
$\eta'_{\eta\pi\pi}\pi^+$	$0.0^{+2.2}_{-0.0}$	28	4.7	$0.0^{+4.9}_{-0.0}$
$\eta'_{\rho\gamma}\pi^+$	$4.4^{+7.2}_{-4.4}$	30	9.0	$5.1^{+8.3}_{-5.1}$
$\eta'_{\eta\pi\pi}\pi^0$	$0.0^{+0.6}_{-0.0}$	23	4.0	$0.0^{+1.5}_{-0.0}$
$\eta'_{\rho\gamma}\pi^0$	$0.8^{+4.1}_{-0.8}$	27	8.3	$1.0^{+5.2}_{-1.0}$
$\eta'_{\eta\pi\pi}K^{*+}_{K^+\pi^0}$	$0.0^{+2.3}_{-0.0}$	14	0.8	0^{+30}_{-0}
$\eta'_{\rho\gamma}K^{*+}_{K^+\pi^0}$	$0.1^{+3.3}_{-0.1}$	9	0.9	1^{+39}_{-1}
$\eta'_{\eta\pi\pi}K^{*+}_{K^0\pi^+}$	$0.0^{+0.6}_{-0.0}$	16	0.6	0^{+10}_{-0}
$\eta'_{\rho\gamma}K^{*+}_{K^0\pi^+}$	$3.2^{+2.9}_{-1.9}$	19	1.3	25^{+23}_{-15}
$\eta'_{\eta\pi\pi}K^{*0}$	$2.4^{+2.7}_{-1.6}$	20	2.3	11^{+12}_{-7}
$\eta'_{\rho\gamma}K^{*0}$	$0.0^{+3.4}_{-0.0}$	21	4.1	$0^{+8.7}_{-0}$
$\eta'_{\eta\pi\pi}\rho^+$	$2.6^{+2.8}_{-1.5}$	15	2.5	11^{+12}_{-6}
$\eta'_{\rho\gamma}\rho^+$	$3.2^{+6.7}_{-3.2}$	9	2.7	12^{+26}_{-12}
$\eta'_{\eta\pi\pi}\rho^0$	$0.0^{+0.9}_{-0.0}$	17	2.9	$0.0^{+3.2}_{-0.0}$
$\eta'_{\rho\gamma}\rho^0$	$2.2^{+4.3}_{-2.2}$	17	5.1	$4.4^{+8.7}_{-4.4}$
$\eta_{\gamma\gamma}K^+$	$5.9^{+6.0}_{-4.6}$	45	17.5	$3.5^{+3.5}_{-2.7}$
$\eta_{3\pi}K^+$	$0.0^{+2.0}_{-0.0}$	29	6.6	$0.0^{+3.1}_{-0.0}$
$\eta_{\gamma\gamma}K^0$	$0.0^{+2.6}_{-0.0}$	38	5.1	$0.0^{+5.2}_{-0.0}$
$\eta_{3\pi}K^0$	$0.0^{+0.9}_{-0.0}$	25	1.9	$0.0^{+5.0}_{-0.0}$
$\eta_{\gamma\gamma}\pi^+$	$5.7^{+5.7}_{-4.6}$	46	18.2	$3.2^{+3.3}_{-2.6}$
$\eta_{3\pi}\pi^+$	$0.0^{+1.1}_{-0.0}$	30	6.8	$0.0^{+1.7}_{-0.0}$
$\eta_{\gamma\gamma}\pi^0$	$0.0^{+1.0}_{-0.0}$	35	13.7	$0.0^{+0.8}_{-0.0}$
$\eta_{3\pi}\pi^0$	$0.0^{+1.4}_{-0.0}$	20	4.6	$0.0^{+3.1}_{-0.0}$
$\eta_{\gamma\gamma}K^{*+}_{K^+\pi^0}$	$9.3^{+5.2}_{-3.5}$	22	2.8	34^{+19}_{-13}
$\eta_{3\pi}K^{*+}_{K^+\pi^0}$	$3.6^{+3.1}_{-2.3}$	15	1.1	32^{+28}_{-20}
$\eta_{\gamma\gamma}K^{*+}_{K^0\pi^+}$	$3.3^{+3.0}_{-2.1}$	25	2.2	16^{+14}_{-10}
$\eta_{3\pi}K^{*+}_{K^0\pi^+}$	$3.0^{+2.7}_{-1.9}$	17	0.9	34^{+30}_{-21}
$\eta_{\gamma\gamma}K^{*0}$	$7.8^{+4.7}_{-3.1}$	32	8.3	$9.7^{+5.8}_{-3.9}$
$\eta_{3\pi}K^{*0}$	$8.0^{+4.4}_{-3.5}$	21	3.3	25^{+14}_{-11}
$\eta_{\gamma\gamma}\rho^+$	$0.0^{+2.5}_{-0.0}$	22	8.5	$0.0^{+3.1}_{-0.0}$
$\eta_{3\pi}\rho^+$	$5.0^{+4.6}_{-3.0}$	15	3.4	15^{+14}_{-9}
$\eta_{\gamma\gamma}\rho^0$	$2.0^{+3.2}_{-2.4}$	26	10.3	$2.0^{+3.3}_{-2.0}$
$\eta_{3\pi}\rho^0$	$2.3^{+4.3}_{-2.3}$	18	4.2	6^{+11}_{-6}

TABLE II. Combined branching fractions (\mathcal{B}_{fit}), significance and final result (\mathcal{B}). The statistical and systematic errors are given for \mathcal{B}_{fit} except where the result is not statistically significant, in which case they are combined and the final result is quoted as a 90% confidence level upper limit. We quote estimates from various theoretical sources [13] for comparison.

Decay mode	$\mathcal{B}_{\text{fit}}(10^{-6})$	Signif. (σ)	$\mathcal{B}(10^{-6})$	Theory $\mathcal{B}(10^{-6})$
$B^+ \rightarrow \eta' K^+$	$80_{-9}^{+10} \pm 7$	16.8	see \mathcal{B}_{fit}	7–65
$B^0 \rightarrow \eta' K^0$	$89_{-16}^{+18} \pm 9$	11.7	see \mathcal{B}_{fit}	9–59
$B^+ \rightarrow \eta' \pi^+$	$1.0_{-1.0}^{+5.8}$	0.0	< 12	1–23
$B^0 \rightarrow \eta' \pi^0$	$0.0_{-0.0}^{+1.8}$	0.0	< 5.7	0.1–14
$B^+ \rightarrow \eta' K^{*+}$	$11.1_{-8.0}^{+12.7}$	1.8	< 35	1–3.7
$B^0 \rightarrow \eta' K^{*0}$	$7.8_{-5.7}^{+7.7}$	1.8	< 24	1–8.0
$B^+ \rightarrow \eta' \rho^+$	$11.2_{-7.0}^{+11.9}$	2.4	< 33	3–24
$B^0 \rightarrow \eta' \rho^0$	$0.0_{-0.0}^{+5.8}$	0.0	< 12	0.1–11
$B^+ \rightarrow \eta K^+$	$2.2_{-2.2}^{+2.8}$	0.8	< 6.9	0.2–5.0
$B^0 \rightarrow \eta K^0$	$0.0_{-0.0}^{+3.2}$	0.0	< 9.3	0.1–3.0
$B^+ \rightarrow \eta \pi^+$	$1.2_{-1.2}^{+2.8}$	0.6	< 5.7	1.9–7.4
$B^0 \rightarrow \eta \pi^0$	$0.0_{-0.0}^{+0.8}$	0.0	< 2.9	0.2–4.3
$B^+ \rightarrow \eta K^{*+}$	$26.4_{-8.2}^{+9.6} \pm 3.3$	4.8	see \mathcal{B}_{fit}	0.2–8.2
$B^0 \rightarrow \eta K^{*0}$	$13.8_{-4.6}^{+5.5} \pm 1.6$	5.1	see \mathcal{B}_{fit}	0.1–8.9
$B^+ \rightarrow \eta \rho^+$	$4.3_{-3.8}^{+5.2}$	1.3	< 15	4–17
$B^0 \rightarrow \eta \rho^0$	$2.6_{-2.6}^{+3.2}$	1.3	< 10	0.1–6.5

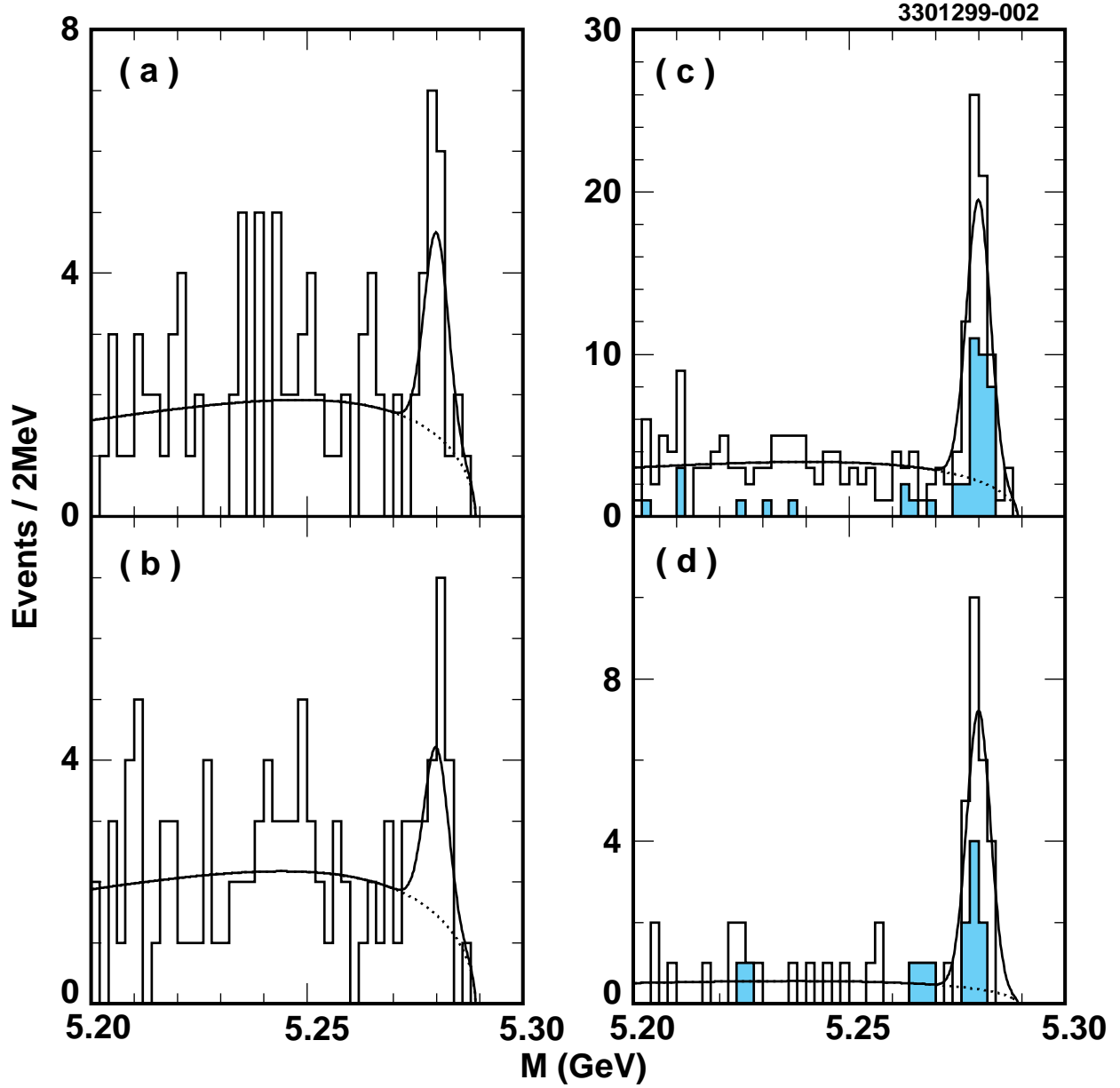


FIG. 2. Projections onto the variable M . The histograms show (a) $B^+ \rightarrow \eta K^{*+}$; (b) $B^0 \rightarrow \eta K^{*0}$; (c) $B^+ \rightarrow \eta' K^+$; (d) $B^0 \rightarrow \eta' K^0$. In (c) and (d) the shaded histograms correspond to the $\eta' \rightarrow \eta \pi \pi$, $\eta \rightarrow \gamma \gamma$ decay chain, while the unshaded histograms correspond to the $\eta' \rightarrow \rho \gamma$ channel. The solid (dashed) line shows the projection for the full fit (background only) with the cut discussed in the text.